IEEE Access
Multidisciplinary | Rapid Review | Open Access Journal

Received November 11, 2020, accepted November 24, 2020, date of publication November 27, 2020,
date of current version December 10, 2020.

Digital Object Identifier 10.1109/ACCESS.2020.3040997

Two-Dimensional Models of Thermoelastic Damping for Out-of-Plane Vibration of Microrings With Circular Cross-Section

YONGPENG TAI[1], NING CHEN[2], JUN XU[2], AND PU LI[3]
[1]College of Automobile and Traffic Engineering, Nanjing Forestry University, Nanjing 210037, China
[2]College of Mechanical and Electronic Engineering, Nanjing Forestry University, Nanjing 210037, China
[3]School of Mechanical Engineering, Southeast University, Nanjing 211189, China

Corresponding author: Yongpeng Tai (tai@njfu.edu.cn)

This work was supported by the Natural Science Foundation of Jiangsu Province of China under Grant BK20160933.

ABSTRACT Thermoelastic damping is an important dissipation mechanism in microresonators. This article presents an analytical model of thermoelastic damping for out-of-plane vibration of microrings with circular cross-section by considering two-dimensional heat conduction. The temperature field of the circular cross-section is calculated by using the Bessel function and free boundary conditions. The coupled motion of bending and torsion in out-of-plane mode has been considered to calculate the mechanical energy. The derivation shows that the analytical expression of thermoelastic damping can be considered as a product of Zener model and the energy ratio of pure bending energy stored to total elastic energy stored. The present model is verified by comparing with the finite-element method. The convergence of the analytical expression has been examined and the characteristics of the expression have been studied by using a normalized form. The effect of geometry on thermoelastic damping has been studied. The results show that thermoelastic damping in microrings of circular cross-section under out-of-plane mode depends on geometry, scales, and vibration frequencies.

INDEX TERMS Microring, out-of-plane vibration, thermoelastic damping, circular cross-section, microresonator.

I. INTRODUCTION

Microring resonator is a typical device of MEMS (microelectromechanical system), which is widely used in MEMS sensors and actuators [1]–[4]. At present, two vibration modes are usually used in the design of ring resonator, i.e., in-plane mode and out-of-plane mode. Using in-plane mode, the ring resonator is suitable to design rate sensors that can detect the angular rate of only one direction [5]–[7]. Using the coupling of in-plane and out-of-plane modes, the ring resonator can be applied to multi-axis rate sensors that can detect the angular rates more than one direction simultaneously [1], [2]. This kind of sensor has attracted the attention of researchers due to higher integration and advanced technology. In fact, microresonators have excellent mechanical properties. However, some dissipation mechanisms, which reduce the performance of the microresonators, become of significance at microscale due to the scale effect. The main dissipation mechanisms include air damping, support loss, and thermoelastic damping. Among them, thermoelastic damping is the intrinsic damping that is produced due to the thermoelastic effect of material and cannot be eliminated by proper design and manufacturing. Therefore, it is very important to investigate the mechanism of thermoelastic damping in microresonators.

Zener [8], [9] first investigated thermoelastic damping in beam resonator of transverse vibration and proposed an analytical model by using the thermal mode superposition method. Zener's study has proved that the analytical model is available not only for a beam with rectangular cross-section but also for that with circular cross-section. Zener model for beam resonator with circular cross-section considers heat conduction in two directions of the section, given by [9]

$$Q^{-1}_{\text{Zener,circular}} = \Delta_E \sum_{q=1}^{\infty} f_q \frac{\omega\tau_q}{1+\omega^2\tau_q^2} \tag{1}$$

The associate editor coordinating the review of this manuscript and approving it for publication was Chaitanya U. Kshirsagar.

where $\Delta_E = E\alpha^2 T_0/C_v$, E is the Young's modulus, T_0 is the ambient temperature, α is the coefficient of thermal expansion, C_v is the heat capacity per unit volume, f_q is the weight coefficient associated with the qth thermal mode, τ_q is the relaxation time and ω is the angular frequency. With the development of MEMS, Zener model has attracted more and more attention, and its validity has been confirmed in resonators of microscale [10]. Lifshitz and Roukes (LR) [11] improved upon Zener model by using a complex temperature field and presented a closed-form expression of thermoelastic damping for a beam resonator with rectangular cross-section. However, LR model is not available for resonators with circular cross-sections.

Based on Zener and LR theory, various models of thermoelastic damping are derived for different structural shapes and vibration modes of microresonators. At present, the thermoelastic damping model has been studied in most common microresonators, such as microbeam [12], microring (in-plane vibration [13]–[16], out-of-plane vibration [17]), and microplate [18], [19]. In some complex microresonators, analytical models of thermoelastic damping are also widely studied and obtained, such as composite laminated structure [20], [21], hemispherical structure [22], etc. However, to our knowledge, most works are focus on the resonator with rectangular cross-section, and only a few works have discussed the models of thermoelastic damping for the case of circular cross-section. This is because the normal methods of micromachining are planar technologies which can be used to fabricate microstructures with rectangular cross-section, and it is difficult to fabricate the structure with circular cross-section using the methods. Under such condition, this work focuses on the theoretical research and has no direct correlation with the current micro-scale technology. On the one hand, there are some works that have already studied the nano/micro-structures with non-rectangular cross-section. With the development of micromachining, the present model can be used for future devices with microring resonators with circular cross-sections. On the other hand, the present model is applicable to but not limited to microstructure, namely, it is also applicable to macrostructure. Therefore, the theory in this article is also effective in other fields and scales.

To date, thermoelastic damping in beam and ring resonators with circular cross-section can be calculated by Zener model and Li's model [14], respectively. However, Li's model is only suitable for the in-plane mode of a ring and cannot predict thermoelastic damping for the case of out-of-plane mode. Although in the previous work [17], we have studied the out-of-plane vibration of a circular ring with rectangular cross-section, the thermoelastic damping of a circular ring with circular cross-section cannot be calculated by the theory of rectangular cross-section due to the fact that the shape of the cross-section has a great influence on the heat conduction. In this article, we derive an analytical model for thermoelastic damping in microring resonators with circular cross-section under out-of-plane vibration. We first solve the two-dimensional heat conduction equation of the circular cross-section and obtain the temperature field of the ring resonator by using the thermal mode superposition method and the properties of the Bessel function. Then, we utilize the definition of the quality factor to derive an analytical expression of thermoelastic damping for out-of-plane vibration of a ring resonator with circular cross-section. The expression can be regarded as a product of Zener model and the energy ratio of pure bending energy stored to total elastic energy stored. The present model is validated by comparing its results with the finite-element method (FEM) solutions.

II. PROBLEM FORMULATION

We consider a microring resonator of uniform circular cross-section under out-of-plane vibration with free boundary conditions as shown in Fig. 1. Three coordinate systems are defined, a global cylindrical coordinate system (R, φ, Z), a local Cartesian coordinate system (x, y, z), and a polar coordinate system (r, β) attached to the circular cross-section where $x = r\sin\beta$ and $z = r\cos\beta$. R_0 and r_0 are the radius of the undeformed centroidal line and the radius of circular cross-section, respectively. u, v, and w are the displacements along the radial, circumferential and axial directions, respectively, and ϕ is the torsional displacement about the y-direction.

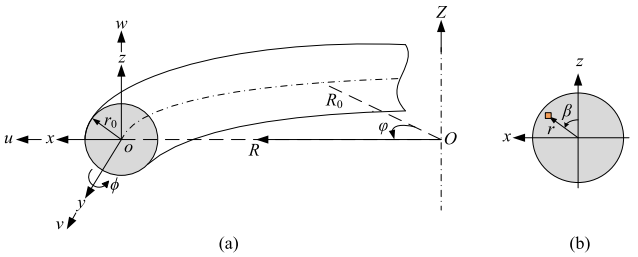

FIGURE 1. Schematic diagram of the circular cross-section of a ring with coordinate systems. (a) The global cylindrical coordinate system (R, φ, Z) and the local Cartesian coordinate system (x, y, z). (b) The polar coordinate system (r, β).

A. COUPLED MOTION OF OUT-OF-PLANE VIBRATION

For the out-of-plane vibration of a ring, the motion is coupling with bending and torsion. The coupling displacements consists of an axial displacement w and a torsional displacement ϕ. Assume that the radius of the cross-section r_0 is small in comparison with the radius of the ring R_0, and hence, warping is neglected. Under such condition, the coupled motion of out-of-plane vibration can be expressed as [2]

$$\begin{cases} w(\varphi, t) = We^{i\omega_n t} = W_0 \cos(n\varphi)\, e^{i\omega_n t} \\ \phi(\varphi, t) = -n^2\zeta We^{i\omega_n t} = -n^2\zeta W_0 \cos(n\varphi)\, e^{i\omega_n t} \end{cases} \tag{2}$$

where W and W_0 represent the amplitude and the maximum amplitude in the axial direction, ω_n is the natural frequency of out-of-plane vibration, n is the mode number ($n = 2, 3, 4\ldots$), and ζ is a parameter, given by

$$\zeta = \frac{1}{R_0}\left[\frac{1+\mu}{1+n^2\mu}\right] \tag{3}$$

where

$$\mu = \frac{GJ}{EI_x} = \frac{1}{1+\upsilon} \tag{4}$$

where G is the shear modulus, J is the torsion constant, I_x is the second moment of area and υ is the Poisson's ratio. For circular cross-section with radius r_0, J and I_x can be expressed as

$$J = 2I_x = \frac{\pi r_0^4}{2} \tag{5}$$

The out-of-plane displacement field of the ring in cylindrical coordinates can be expressed as [23], [24]

$$\begin{cases} u(R,\varphi,Z,t) = z\phi \\ v(R,\varphi,Z,t) = -z\dfrac{\partial w}{R\partial\varphi} \\ w(R,\varphi,Z,t) = w(\varphi,t) \end{cases} \tag{6}$$

B. STRAIN AND STRESS FIELDS

For the thin ring ($r_0 \ll R_0$), the differences of strains along the radius direction on the cross-section can be neglected. Therefore, using (2), (6) and the relevance between w and ϕ, the strain field of the ring is obtained and can be expressed in polar coordinate [17], [25]

$$\begin{cases} \varepsilon_\varphi = \dfrac{u}{R_0} + \dfrac{1}{R_0}\dfrac{\partial v}{\partial\varphi} = -r\cos\beta\dfrac{1-R_0\zeta}{R_0^2}\dfrac{\partial^2 w}{\partial\varphi^2} \\ \varepsilon_R = \varepsilon_Z = -\upsilon\varepsilon_\varphi + (1+\upsilon)\,\varepsilon_{\text{thermal}} \\ \gamma_{R\varphi} = \dfrac{1}{R_0}\dfrac{\partial u}{\partial\varphi} - \dfrac{v}{R_0} = r\cos\beta\dfrac{1-n^2R_0\zeta}{R_0^2}\dfrac{\partial w}{\partial\varphi} \\ \gamma_{\varphi Z} = -\dfrac{x}{R_0}\left(\dfrac{\partial\phi}{\partial\varphi} + \dfrac{\partial w}{R_0\partial\varphi}\right) = -r\sin\beta\dfrac{1-n^2R_0\zeta}{R_0^2}\dfrac{\partial w}{\partial\varphi} \\ \gamma_{RZ} = 0 \end{cases} \tag{7}$$

where $\varepsilon_{\text{thermal}} = \alpha\theta$ represents the thermal strain caused by thermoelastic effect and θ is the change in temperature.

Typically, the temperature change caused by the thermoelastic effect is relatively small. Therefore, compared with the mechanical stresses, the thermal stress produced by θ can be ignored [26]. Then, the stress filed of the ring can be expressed as

$$\begin{cases} \sigma_\varphi = E\varepsilon_\varphi = -Er\cos\beta\dfrac{1-R_0\zeta}{R_0^2}\dfrac{\partial^2 w}{\partial\varphi^2} \\ \tau_{r\varphi} = G\gamma_{r\varphi} = \dfrac{Er\cos\beta}{2(1+\upsilon)}\dfrac{1-n^2R_0\zeta}{R_0^2}\dfrac{\partial w}{\partial\varphi} \\ \tau_{\varphi Z} = G\gamma_{\varphi Z} = -\dfrac{Er\sin\beta}{2(1+\upsilon)}\dfrac{1-n^2R_0\zeta}{R_0^2}\dfrac{\partial w}{\partial\varphi} \end{cases} \tag{8}$$

C. HEAT CONDUCTION EQUATION

Assume that the ring is subjected to time-harmonic force with the natural frequency ω_n and then operates in out-of-plane vibration. The steady-state responses of the translation displacement and the relative temperature filed in the ring have the form

$$\begin{cases} w(\varphi,t) = W(\varphi)\,e^{\mathrm{i}\omega_n t} = W_0\cos(n\varphi)\,e^{\mathrm{i}\omega_n t} \\ \theta(x,\varphi,z,t) = \theta_0(x,\varphi,z)\,\mathrm{e}^{\mathrm{i}\omega_n t} \end{cases} \tag{9}$$

According to the Fourier Law, the thermoelastic temperature field is governed by the heat conduction equation, given by [27]

$$\frac{\partial\theta}{\partial t} = \chi\nabla^2\theta - \frac{E\alpha T_0}{(1-2\upsilon)C_v}\frac{\partial}{\partial t}\sum_j \varepsilon_{jj} \tag{10}$$

where $\nabla^2(\bullet)$ represents the Laplacian operator and ε_{jj} is the normal strain. In fact, the bending component of out-of-plane vibration is the main cause of thermoelastic damping whereas the torsion component causes no local volume change and hence, suffers no damping [11]. For bending vibration, most heat flow transports along transverse directions (x- and z-axes). Accordingly, we assume that the heat flow along circumferential direction φ is neglected. For such case, ∇^2 can be expressed as

$$\nabla^2 = \frac{\partial^2}{\partial x^2} + \frac{\partial^2}{\partial z^2} = \frac{\partial^2}{\partial r^2} + \frac{1}{r}\frac{\partial}{\partial r} + \frac{1}{r^2}\frac{\partial^2}{\partial\beta^2} \tag{11}$$

Therefore, we obtain a two-dimensional heat conduction equation, given by

$$\begin{aligned} \frac{\partial\theta}{\partial t} = \chi\left(\frac{\partial^2\theta}{\partial r^2} + \frac{1}{r}\frac{\partial\theta}{\partial r} + \frac{1}{r^2}\frac{\partial^2\theta}{\partial\beta^2}\right) \\ + r\cos\beta\frac{\Delta_E}{\alpha}\frac{\partial}{\partial t}\left(\frac{1-R\xi}{R^2}\frac{\partial^2 w}{\partial\varphi^2}\right) \end{aligned} \tag{12}$$

The last term on the right side of the above equation is the internal heat source excitation. When the excitation is 0, we obtain a two-dimensional free heat conduction equation on a circular surface, given by

$$\frac{\partial\theta}{\partial t} = \chi\left(\frac{\partial^2\theta}{\partial r^2} + \frac{1}{r}\frac{\partial\theta}{\partial r} + \frac{1}{r^2}\frac{\partial^2\theta}{\partial\beta^2}\right) \tag{13}$$

Equation (13) is a typical heat conduction equation of a circular plane. It is very mature to solve the eigenvalue and thermal mode of the equation by using the separation of variables method, and the form of the solution can be expressed as a sum of products of a thermal mode equation θ_1, a spatial frequency equation θ_2 and a time-frequency equation θ_3, given by

$$\theta(r,\beta,\varphi,t) = \theta_1(r,\varphi)\,\theta_2(\beta)\,\theta_3(t) \tag{14}$$

where θ_1 is a Bessel function of the first kind.

III. SOLUTION OF THE HEAT CONDUCTION EQUATION

A. TEMPERATURE FIELD

The thermoelastic effect during vibration of the resonator results in the internal heat source, that is, the excitation of heat conduction. For (12), the last term on the right is the heat source term of the system, which excites the system with a time-frequency ω_n from $\exp(\mathrm{i}\omega_n t)$ and a spatial frequency

$\omega_k = 1$ from $\cos\beta$. Therefore, based on (14), the steady-state response of the temperature field can be expressed using the mode superposition method, given by

$$\begin{aligned}\theta(r,\beta,\varphi,t) &= \theta_0(r,\beta,\varphi)\, e^{i\omega_n t} \\ &= \sum_{q=1}^{\infty} c_q J_1(\gamma_q r)\cos\beta e^{i\omega_n t}\end{aligned} \tag{15}$$

where γ_p is a positive number and c_q is the weight coefficient for different thermal modes, which can be determined by boundary conditions of heat conduction.

Assume that no heat transfer from the ring to the environment. The adiabatic boundary conditions are employed, i.e., $\partial\theta_0/\partial r = 0$ at $r = \pm r_0$. Substituting (15) into the boundary conditions, yields

$$\left.\frac{\partial\theta_0}{\partial r}\right|_{r=r_0} = \sum_{q=1}^{\infty} c_q \frac{d}{dr} J_1(\gamma_q r_0)\cos\beta = 0 \tag{16}$$

Using the properties of the Bessel function, we obtain

$$J_0(a_q) - J_2(a_q) = 0 \; or \; J_1(a_q) = a_q J_0(a_q) \tag{17}$$

where $a_q = \gamma_q r_0$ is the root of (17).

Substituting (15) into (12), we obtain the distribution equation of temperature field (see **APPENDIX A** for details)

$$\sum_{q=1}^{\infty} c_q\left(\gamma_q^2 + \frac{i\omega_n}{\chi}\right) J_1(\gamma_q r) = r\frac{i\omega_n}{\chi}\frac{\Delta_E}{\alpha}\frac{1-R_0\xi}{R_0^2}\frac{\partial^2 W}{\partial\varphi^2} \tag{18}$$

To solve the coefficient c_q, the weighted orthogonality of the Bessel function is used, given by

$$\int_0^{r_0} r J_1(\gamma_p r) J_1(\gamma_q r)\, dr = 0, \quad \text{when } p \neq q \tag{19}$$

Let both sides of (18) be multiplied by $rJ_1(\gamma_p\beta)$ and integrated from $r = 0$ to r_0, and hence, we obtain

$$\begin{aligned}c_q\left(\gamma_q^2 + \frac{i\omega_n}{\chi}\right)\int_0^{r_0} r J_1^2(\gamma_q r)\, dr \\ = \frac{i\omega_n}{\chi}\frac{\Delta_E}{\alpha}\frac{1-R_0\xi}{R_0^2}\frac{\partial^2 W}{\partial\varphi^2}\int_0^{r_0} r^2 J_1(\gamma_q r)\, dr\end{aligned} \tag{20}$$

Utilizing the boundary conditions (17), we can solve the above equation directly and then the coefficient c_q is obtained as (see **APPENDIX A** for details)

$$c_q = \frac{2\Delta_E r_0\left(\omega_n^2 + i\omega_n\chi\gamma_q^2\right)}{\left(\chi^2\gamma_q^4 + \omega_n^2\right)\left(a_q^2 - 1\right)\alpha J_1(a_q)}\frac{1-R_0\xi}{R_0^2}\frac{\partial^2 W}{\partial\varphi^2} \tag{21}$$

Note that c_q is a complex number that represents the out of phase relationship between temperature field and elastic vibration caused by thermoelastic damping.

B. THERMOELASTIC DAMPING

According to the definition of quality factor Q, thermoelastic damping can be expressed as

$$Q^{-1} = \frac{1}{2\pi}\frac{\Delta W}{W_{\text{stored}}} \tag{22}$$

where ΔW is the energy loss per cycle due to thermoelastic damping and W_{stored} is the maximum energy stored per cycle of vibration. For vibrating resonators, ΔW is related to the coupling between stress field and thermal strain field that results in the conversion of mechanical energy into heat energy, given by

$$\Delta W = -\pi\iiint_V \hat{\sigma}_\varphi Im\left(\hat{\varepsilon}_{\text{thermal}}\right) dV \tag{23}$$

where the hat (^) denotes the amplitude and the imaginary part of thermal strain can be expressed as

$$\begin{aligned}\text{Im}\left(\hat{\varepsilon}_{\text{thermal}}\right) &= \alpha\,\text{Im}(\theta_0) \\ &= \alpha\cos\beta\sum_{q=1}^{\infty}\text{Im}(c_q) J_1(\gamma_q r)\end{aligned} \tag{24}$$

For out-of-plane vibration, W_{stored} is caused by the coupled motion of bending and torsion, given by

$$W_{\text{stored}} = \frac{1}{2}\iiint_V\left(\hat{\sigma}_\varphi\hat{\varepsilon}_\varphi + \hat{\tau}_{r\varphi}\hat{\gamma}_{r\varphi} + \hat{\tau}_{\varphi Z}\hat{\gamma}_{\varphi Z}\right) dV \tag{25}$$

Substituting (7) and (8) into (23) and (25), the energy loss produced per cycle and the maximum energy stored per cycle can be expressed as (see **APPENDIX B** for details)

$$\begin{aligned}\Delta W &= 2\pi^3 E\Delta_E\omega_n\chi n^4 W_0^2 \\ &\quad\times\cdot\frac{r_0^2}{R_0^3}\frac{\left(n^2-1\right)^2\mu^2}{\left(1+n^2\mu\right)^2}\sum_{q=1}^{\infty}\frac{1}{\left(\chi^2\gamma_q^4+\omega_n^2\right)\left(a_q^2-1\right)}\end{aligned} \tag{26}$$

$$W_{\text{stored}} = \frac{E\pi^2 r_0^4}{8R_0^3}n^4 W_0^2\frac{\left(n^2-1\right)^2\mu^2}{\left(1+n^2\mu\right)^2}\left[1 + \frac{1}{(1+\upsilon)n^2\mu^2}\right] \tag{27}$$

Substituting (26) and (27) into (22), and using (4), the thermoelastic damping model for out-of-plane vibration of a ring with circular cross-section can be expressed as

$$Q^{-1} = \frac{1}{1+(1+\upsilon)/n^2}\Delta_E\sum_{q=1}^{\infty} f_q\frac{\omega_n\tau_q}{1+\omega_n^2\tau_q^2} \tag{28}$$

where f_q is the weight coefficient and τ_q is the relaxation time, given by

$$f_q = \frac{8}{a_q^2\left(a_q^2-1\right)}\tau_q = \frac{r_0^2}{a_q^2\chi} \tag{29}$$

According to (1), (28) can also be expressed as

$$Q^{-1} = \frac{1}{1+(1+\upsilon)/n^2}Q^{-1}_{\text{Zener,circular}} \tag{30}$$

Additionally, utilizing the energy expression, we can obtain the energy ratio

$$\frac{W_{\text{bending}}}{W_{\text{stored}}} = \frac{1}{1+(1+\upsilon)/n^2} \tag{31}$$

where W_{bending} is the pure bending energy stored related to the bending component of the coupled motion. Thus, Q^{-1} can be regarded as the product of the Zener model and the energy ratio of pure bending energy stored to total elastic energy stored.

C. SIMPLIFIED MODEL

Table 1 lists the values of the weight coefficient f_q for different thermal modes. Note that high order modes ($q = 2, 3, 4\ldots$) can be neglected by introducing a very little error. Hence, we remain only the first term ($q = 1$) in the summation of (28), and then the simplified model of thermoelastic damping can be expressed as

$$Q^{-1} = \frac{1}{1+(1+\upsilon)/n^2}\Delta_E \frac{\omega_n \tau}{1+\omega_n^2\tau^2} \tag{32}$$

where $\tau = \tau_1 = 0.295 r_0^2/\chi$. The relaxation time of circular cross-section τ is different from that of square cross-section τ_{square}, given by [9], [11]

$$\tau_{\text{sqrare}} = \frac{b^2}{\pi^2 \chi} \tag{33}$$

where b is the beam thickness. When $b = 0.5431\pi r_0$, we obtain $\tau_{\text{square}} = \tau$. Fig. 2 shows a comparison between τ_{square} and τ for three different cases. From the figure, it shows that $\tau_{\text{square}} > \tau$, when the diameter of the circular section is equal to b ($b = 2r_0$), or the two kinds of sections are of the same area ($b = \pi^{0.5} r_0$). Also shown in the figure, $\tau_{\text{square}} < \tau$, when r_0 is the circumscribed circle of the square ($b = 2^{0.5} r_0$).

TABLE 1. The values of a_q and f_q for the first six thermal modes.

Item	Value					
q	1	2	3	4	5	6
a_q	1.841	5.331	8.536	11.706	14.864	18.016
f_q	0.987	1.03E-2	1.53E-3	4.29E-4	1.65E-4	7.62E-5

Note that the thermoelastic damping model (30) is similar to that for rectangular sections in the reference [17]. However, the two equations are only similar in form and cannot be substituted for each other. Through comparison, we find that different cross-section shapes lead to different heat conduction paths besides the mechanical parameters such as the torsional constant J and the second moment of area I_x. This is also the main reason why the model for rectangular cross-section in the reference [17] cannot be used for circular cross-section. In this article, a two-dimensional heat conduction equation is adopted for circular cross-section, which considers the heat flow in the radial and axial directions (x- and z-axes),

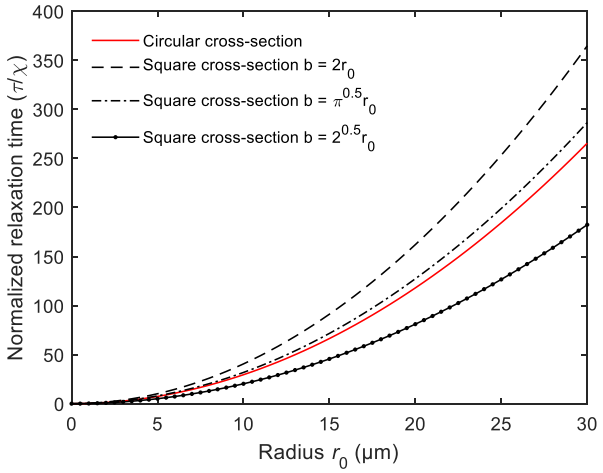

FIGURE 2. Variation of normalized relaxation time with r_0.

while the equation of rectangular cross-section [17] only considers the heat flow in the axial direction. Theoretically, the two-dimensional heat conduction model has higher accuracy than the one-dimensional one, but it is more difficult to obtain the analytical solution. However, for circular cross-section, the two-dimensional heat conduction equation is easier to solve than the one-dimensional heat conduction equation. Therefore, for the circular cross-section, we use the two-dimensional heat conduction equation with higher accuracy to describe the internal heat transfer phenomenon. On the contrary, for rectangular cross-section, it is easier to obtain the analytical solution of one-dimensional heat conduction equation with sufficient accuracy, because most of the heat conduction occurs in one direction.

IV. RESULTS

In this section, we first verify the validity of the present model by comparing with FEM results. Then, the convergence of the present model as well as its characteristics of normalized expression are examined carefully. Next, the effect of ring geometry on thermoelastic damping is studied. Last, the differences of thermoelastic damping in the rings with circular cross-section and square cross-section are discussed. The material properties used for the theoretical calculation of this section are list in Table 2.

TABLE 2. Material properties of polysilicon at 300 K [28].

Parameters	Polysilicon
Young's modulus, E (GPa)	157
Poisson's ratio, υ	0.22
Density, ρ (kg m^{-3})	2330
Thermal conductivity, κ (W m^{-1} K^{-1})	90
Specific heat, C_p (J kg^{-1} K^{-1})	699
Thermal expansion coefficient, α (K^{-1})	2.6×10^{-6}

A. VERIFICATION

In this section, the present model of thermoelastic damping is verified by comparing with FEM. The present model is

a two-dimensional model considering the heat flow along axial and radial directions. Theoretically, FEM is a very high accurate method to predict thermoelastic damping because three-dimensional heat conduction is considered in FEM. The FEM simulation results are obtained by using free boundary conditions and harmonic exciting force of axial direction applied to a small area of the ring.

Fig. 3 shows the imaginary part of the temperature of the ring vibrating in out-of-plane mode $n = 2$. The specifications of the ring are $r_0 = 10\ \mu$m and $R_0 = 200\ \mu$m. The imaginary part of the temperature represents the part of the material temperature that is out of phase with the mechanical vibration. As shown in the figure, the temperature gradient of the cross-section is mainly along the axial direction, but the role of radial direction cannot be ignored.

Fig. 4 shows the comparison of thermoelastic damping obtained by FEM and the present model for different structure dimensions and natural frequencies. The critical parameters are $r_0 = 10\ \mu$m and $R_0 = 200\ \mu$m, 600 μm, and 1000 μm. As shown in Fig. 4, the results of the present model are in good agreement with those of FEM for all cases. Note that the present model with $q = 10$ is more accurate than the case of $q = 1$. However, the difference between the two cases of $q = 1$ and $q = 10$ is negligibly small. Fig. 5 shows the relative errors between the results of FEM and the present model. As shown in the figure, the analytical results obtained using $q = 10$ are closer to FEM than those using $q = 1$. For all cases, the maximum error of the present model is within 15% and 4% for $q = 1$ and $q = 10$, respectively. Also shown in the figure, for the case of thin ring (i.e., a large ratio of R_0/r_0), the present model exhibits very high accuracy. However, for the case of $R_0/r_0 = 20$, the relative error is remarkable at high order mode.

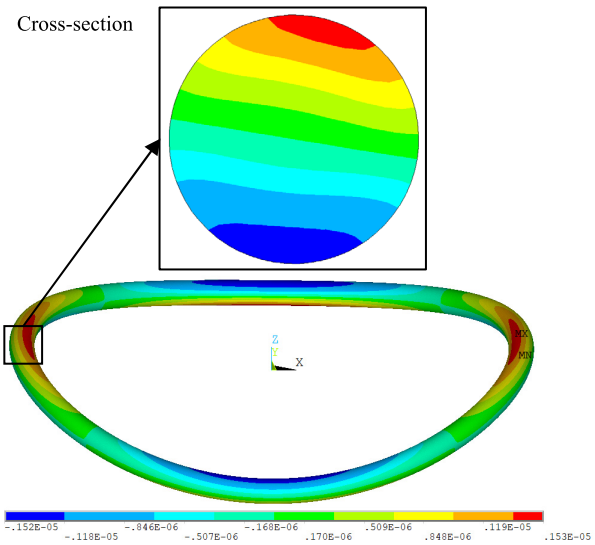

FIGURE 3. The imaginary part of the temperature field of a ring resonator in out-of-plane mode ($n = 2$). The inset is the temperature distribution of circular cross-section.

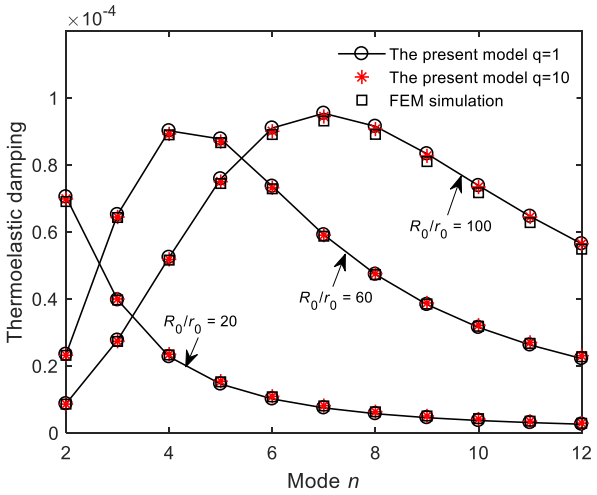

FIGURE 4. Comparison between the results obtained by FEM and the present model with constant $r_0 = 10\ \mu$m.

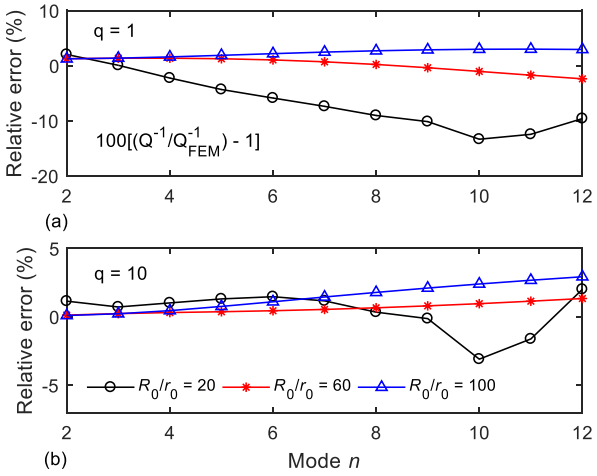

FIGURE 5. The relative error of thermoelastic damping between FEM and the present model for different modes. (a) $q = 1$. (b) $q = 10$.

B. CONVERGENCE OF THE THERMOELASTIC DAMPING EQUATION

The convergence of the thermoelastic damping equation in this article is checked carefully. Fig. 6 shows thermoelastic damping calculated by the analytical model (28) for the cases of $q = 1$, 2, 5, 10, and 20. The resonator dimensions are $r_0 = 10\ \mu$m and $R_0 = 100\ \mu$m. As shown in the figure, the curve of $q = 1$ almost coincides with that of $q = 20$ at low order modes. The curve of $q = 2$ is sufficient precision at mode $n = 20$ but not in good agreement with that of $q = 20$ at mode $n = 30$. Note that the curve of $q = 5$ is in excellent agreement with that of $q = 20$ even at very high order modes. Thus, the convergence can be achieved by using $q = 1$ or $q = 5$ for low or high order modes, respectively.

C. NORMALIZED EQUATION OF THERMOELASTIC DAMPING

To study the characteristics of the model of thermoelastic damping derived in this article, we normalize (32) and transform it into a Lorentzian with normalized frequency $\eta = \omega_n \tau$,

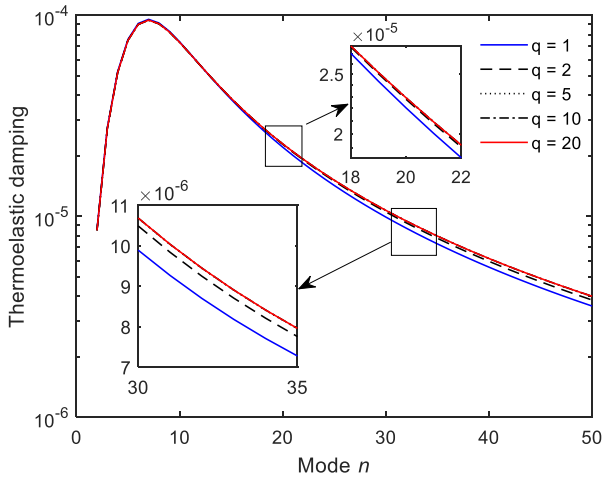

FIGURE 6. Thermoelastic damping calculated by the present model for different q.

given by

$$\frac{Q^{-1}}{\Delta_E} = \frac{1}{1+(1+\upsilon)/n^2} L(\eta) \tag{34}$$

where $L(\cdot)$ is the Lorentzian, given by

$$L(\eta) = \frac{\eta}{1+\eta^2} \tag{35}$$

For any value of η, the boundaries of Q^{-1}/Δ_E can be expressed as

$$\frac{1}{1+(1+\upsilon)/4} L(\eta) \le \frac{Q^{-1}}{\Delta_E} \le L(\eta) \tag{36}$$

Fig. 7 shows the normalized thermoelastic damping varying with η for the cases of $n = 2$, 5, 10, and ∞. The curves of $n = 2$ and ∞ are the boundaries as expected in (36). As shown in Fig. 7, Debye peak exists when η equals to 1. The inset shows the Debye peaks for different mode numbers n. It illustrates that increasing mode number n increases the value of Debye peak. Moreover, at any frequency, the larger the mode number n, the larger the thermoelastic damping value. Note that the curve of n =10 is very close to that of $n = \infty$. Therefore, for the high order mode of out-of-plane vibration, the thermoelastic damping value of a ring is approaching to that of a beam with circular cross-section in transverse vibration.

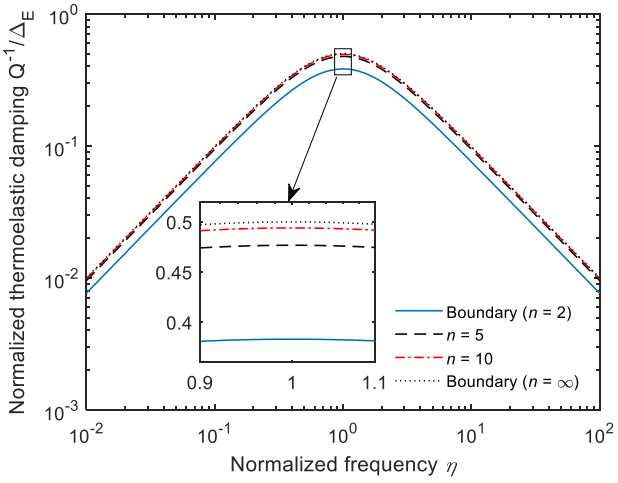

FIGURE 7. Variation of normalized thermoelastic damping with the dimensionless variable $\eta = \omega_n \tau$.

D. EFFECT OF GEOMETRY

In this section, the effect of structure dimensions of ring resonators on thermoelastic damping is studied for different modes and ratios R_0/r_0. Fig. 8 shows the dependence of thermoelastic damping on mode number n with constant r_0 = 10 μm for different R_0. As shown in Fig. 8, increasing the value of R_0 increases the mode number n which is associated with the Debye peak.

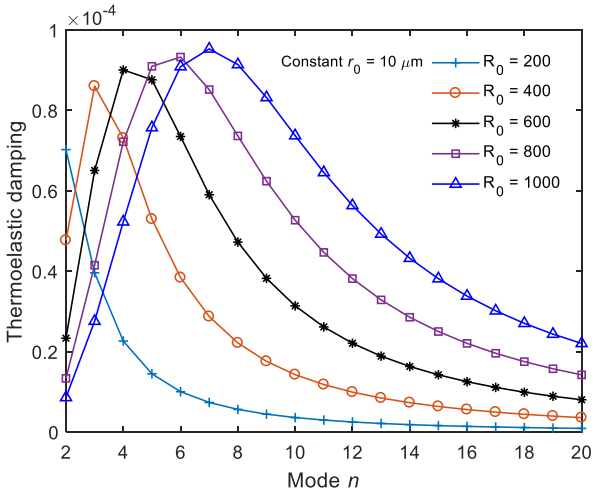

FIGURE 8. Dependence of thermoelastic damping on mode number n with constant r_0 = 10 μm for different R_0.

For ring resonators with circular cross-section, R_0 and r_0 are two key geometric dimensions. Fig. 9 shows the dependence of thermoelastic damping on varying ratios R_0/r_0 with constant R_0 = 1000 μm for the cases of n = 2 to 6. As shown in the figure, for any case, a peak value exists when changing the ratio R_0/r_0. On both sides of the peak, the curve changes monotonically with the increase of R_0/r_0. Also shown in the figure, the ratio R_0/r_0, corresponding to the peak value, increases with increasing mode number n.

Fig. 10 shows thermoelastic damping varying with the radius r_0 for constant R_0/r_0 = 40. As shown in this figure, there is a peak value of thermoelastic damping which corresponds to a certain r_0 for each curve of mode number n. As the increase of n, the radius r_0, corresponding to the peak value, is getting smaller.

E. COMPARISON BETWEEN CIRCULAR AND SQUARE CROSS-SECTIONS

The microring resonators with rectangular cross-section have already been widely used in the MEMS field. In this section,

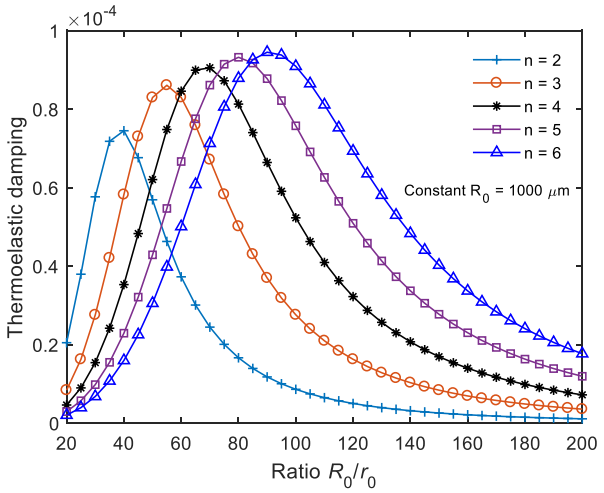

FIGURE 9. Dependence of thermoelastic damping on varying ratios R_0/r_0 with constant $R_0 = 1000$ μm for different n.

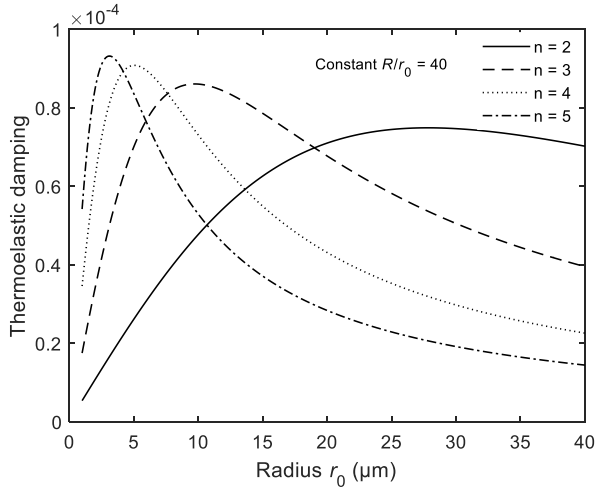

FIGURE 10. Dependence of thermoelastic damping on varying r with constant $R/r = 40$.

we compare the results of thermoelastic damping between circular and square cross-sections under the same area of cross-sections ($b = \pi^{0.5} r_0$).

Fig. 11 shows the ratio of thermoelastic damping of square section ring to circular section ring. The value of R_0/r_0 is fixed to 40. As shown in this figure, the ratio varies with mode numbers and scales, and a minimum value of the ratio exists (> 0.9) for all cases of r_0. In the regime of high order mode, the ratio increases monotonically with the increasing of mode number n. Also shown in the figure, the differences of thermoelastic damping between circular and square cross-sections are not larger than 10% under such conditions. As can be seen from the figure, thermoelastic damping in circular cross-section is different from those in square cross-section and it is difficult to find a regular relationship between the two kinds of cross-sections. This is due to the different cross-section shapes that affect the modal frequency and heat conduction. Therefore, it is necessary to establish a

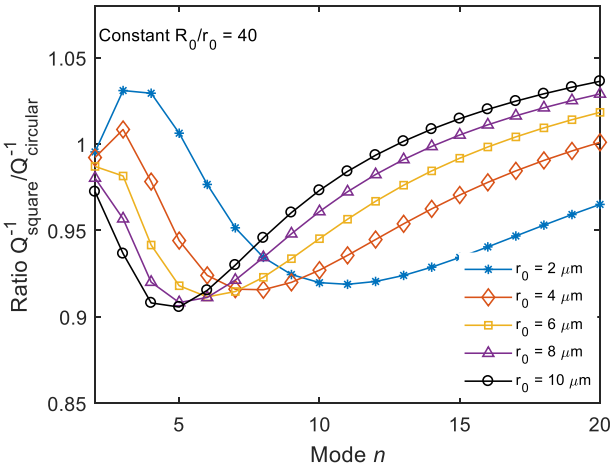

FIGURE 11. The ratio of thermoelastic damping of square section ring to circular section ring for the case of equal cross-sectional area.

new thermoelastic damping model for microresonators when the shape of the cross-section and the vibration mode are changed.

V. CONCLUSION

We presented an analytical model for thermoelastic damping in microring resonators with circular cross-section under out-of-plane vibration. We applied the mode superposition method to solve the heat conduction equation for two-dimensional heat flow across the circular cross-section and obtained the temperature field of the ring. The validity of the present model is verified by comparing with the FEM simulation. It is found that the results of the present model are in good agreement with those of FEM. The convergence of the present model is carefully checked and the characteristics of the present model are studied by using the normalized equation. The geometry effects on thermoelastic damping had been investigated for different ratios R_0/r_0 and scales. By comparison, it is found that the differences of thermoelastic damping between circular and square cross-sections under the same area of cross-sections depend on the mode number and size scale.

APPENDIX A
SOLUTION OF TEMPERATURE FIELD

Substituting (15) into (12), we obtain

$$\sum_{q=1}^{\infty} c_q \left[J_1''(\gamma_q r) + \frac{1}{r} J_1'(\gamma_q r) - \frac{1}{r^2} J_1(\gamma_q r) - \frac{i\omega_n}{\chi} J_1(\gamma_q r) \right] = -r \frac{i\omega_n}{\chi} \frac{\Delta_E}{\alpha} \frac{1 - R_0\xi}{R_0^2} \frac{\partial^2 W}{\partial \varphi^2} \quad \text{(A.1)}$$

According to the characteristics of the Bessel function, we obtain

$$J_1''(\gamma_q r) + \frac{1}{r} J_1'(\gamma_q r) - \frac{1}{r^2} J_1(\gamma_q r) - \frac{i\omega_n}{\chi} J_1(\gamma_q r) = -\left(\gamma_q^2 + \frac{i\omega_n}{\chi} \right) J_1(\gamma_q r) \quad \text{(A.2)}$$

Then, (A.1) can be expressed as

$$\sum_{q=1}^{\infty} c_q \left(\gamma_q^2+\frac{i\omega_n}{\chi}\right) J_1\left(\gamma_q r\right)=r\frac{i\omega_n}{\chi}\frac{\Delta_E}{\alpha}\frac{1-R_0\xi}{R_0^2}\frac{\partial^2 W}{\partial\varphi^2} \quad (A.3)$$

Using (19), we transform the above equation into the form as (20). The integrations in (20) can be solved, given by

$$\int_0^{r_0} rJ_1^2\left(\gamma_q r\right)dr = \left\|J_1\left(\gamma_q r\right)\right\|^2 = \frac{r_0^2}{2}\left(\frac{d}{dr}J_1\left(a_q\right)\right)^2+\frac{1}{2}\left(r_0^2-\frac{1}{\gamma_q^2}\right)J_1^2\left(a_q\right) \quad (A.4)$$

$$\int_0^{r_0} r^2 J_1\left(\gamma_p r\right)dr = \frac{r_0^2}{\gamma_q}J_2\left(a_q\right) \quad (A.5)$$

Based on the boundary conditions (17), (A.4) and (A.5) can be expressed as

$$\int_0^{r_0} rJ_1^2\left(\gamma_q r\right)dr = \frac{1}{2}\left(r_0^2-\frac{1}{\gamma_q^2}\right)J_1^2\left(a_q\right) \quad (A.6)$$

$$\int_0^{r_0} r^2 J_1\left(\gamma_p r\right)dr = \frac{r_0^2}{a_q\gamma_q}J_1\left(a_q\right) \quad (A.7)$$

Substituting (A.6) and (A.7) into (20), yields

$$c_q\left(\gamma_q^2+\frac{i\omega_n}{\chi}\right)\frac{1}{2}\left(r_0^2-\frac{1}{\gamma_q^2}\right)J_1\left(a_q\right) = \frac{i\omega_n}{\chi}\frac{\Delta_E}{\alpha}\frac{1-R_0\xi}{R_0^2}\frac{\partial^2 W}{\partial\varphi^2}\frac{r_0^2}{a_q\gamma_q} \quad (A.8)$$

By solving the above equation, c_q can be obtained as (21).

APPENDIX B
ENERGY CALCULATION

Using (8), (23) and thermal strain expression $\varepsilon_{\text{thermal}} = \alpha\theta$, the energy loss per cycle over the entire structure is

$$\begin{aligned}\Delta W &= -\pi\iiint_V \hat{\sigma}_\varphi\alpha\cos\beta\sum_{q=1}^{\infty}\text{Im}\left(c_q\right)J_1\left(\gamma_q r\right)dV\\ &= 2\pi E\Delta_E\omega\chi r_0\frac{(1-R_0\xi)^2}{R_0^4}\\ &\quad\times\sum_{q=1}^{\infty}\frac{\gamma_q^2}{\left(\chi^2\gamma_q^4+\omega_n^2\right)\left(a_q^2-1\right)J_1\left(a_q\right)}\\ &\quad\cdot\iiint_V r^2J_1\left(\gamma_q r\right)\cos^2\beta\left(\frac{\partial^2 W}{\partial\varphi^2}\right)^2(R_0+r\sin\beta)\,dr d\beta d\varphi\end{aligned} \quad (B.1)$$

The integration in (B.1) can be solved, given by

$$\begin{aligned}&\iint_V r^2J_1\left(\gamma_q r\right)\cos^2\beta\left(\frac{\partial^2 W}{\partial\varphi^2}\right)^2(R_0+r\sin\beta)\,dr d\beta d\varphi\\ &= \int_0^{2\pi}\left(\frac{\partial^2 W}{\partial\varphi^2}\right)^2 d\varphi\left[R_0\int_0^{r_0}r^2J_1\left(\gamma_q r\right)dr\cdot\int_0^{2\pi}\cos^2\beta d\beta\right.\\ &\quad\left.+\int_0^{r_0}r^3J_1\left(\gamma_q r\right)dr\int_0^{2\pi}\cos^2\beta\sin\beta d\beta\right]\\ &= R_0\int_0^{r_0}r^2J_1\left(\gamma_q r\right)dr\cdot\int_0^{2\pi}\cos^2\beta d\beta\cdot\int_0^{2\pi}\left(\frac{\partial^2 W}{\partial\varphi^2}\right)^2 d\varphi\\ &= \frac{r_0R_0\pi^2W_0^2n^4}{\gamma_q^2}J_1\left(a_q\right)\end{aligned} \quad (B.2)$$

Thus, using (3) and (B.2), ΔW can be written as (26).

Substituting (7) and (8) into (25), the maximum energy stored per cycle is given by

$$\begin{aligned}W_{\text{stored}} &= \frac{E}{2}\frac{(1-R_0\zeta)^2}{R_0^4}\\ &\quad\cdot\iint r^3\cos^2\beta\,(R_0+r\sin\beta)\,dr d\beta\cdot\int\left(\frac{\partial^2 W}{\partial\varphi^2}\right)^2 d\varphi\\ &\quad+\frac{E}{4(1+\upsilon)}\frac{\left(1-n^2R_0\zeta\right)^2}{R_0^4}\\ &\quad\cdot\iint r^3\cos^2\beta\,(R_0+r\sin\beta)\,dr d\beta\cdot\int\left(\frac{\partial W}{\partial\varphi}\right)^2 d\varphi\\ &\quad+\frac{E}{4(1+\upsilon)}\frac{\left(1-n^2R_0\zeta\right)^2}{R_0^4}\\ &\quad\cdot\iint r^3\sin^2\beta\,(R_0+r\sin\beta)\,dr d\beta\cdot\int\left(\frac{\partial W}{\partial\varphi}\right)^2 d\varphi\\ &= \frac{E\pi^2r_0^4}{8R_0^3}n^4W_0^2\left[(1-R\zeta)^2+\frac{\left(1-n^2R\zeta\right)^2}{(1+\upsilon)\,n^2}\right]\end{aligned} \quad (B.3)$$

Finally, using (3), W_{stored} can be expressed as (27).

REFERENCES

[1] A. K. Rourke, S. McWilliam, and C. H. J. Fox, "Frequency trimming of a vibrating ring-based multi-axis rate sensor," *J. Sound Vib.*, vol. 280, nos. 3–5, pp. 495–530, Feb. 2005.
[2] R. Eley, C. H. J. Fox, and S. Mcwilliam, "Coriolis coupling effects on the vibration of rotating rings," *J. Sound Vib.*, vol. 238, no. 3, pp. 459–480, Nov. 2000.
[3] R. Eley, C. H. J. Fox, and S. McWilliam, "The dynamics of a vibrating-ring multi-axis rate gyroscope," *Proc. Inst. Mech. Eng., C, J. Mech. Eng. Sci.*, vol. 214, no. 12, pp. 1503–1513, Dec. 2000.
[4] M.-H. Li, C.-Y. Chen, C.-S. Li, C.-H. Chin, and S.-S. Li, "Design and characterization of a dual-mode CMOS-MEMS resonator for TCF manipulation," *J. Microelectromech. Syst.*, vol. 24, no. 2, pp. 446–457, Apr. 2015.
[5] Z. L. Hao and F. Ayazi, "Thermoelastic damping in flexural-mode ring gyroscopes," *Micro-Electro-Mech. Syst. -*, vol. 2005, vol. 7, pp. 335–343, 2005.
[6] J.-H. Kim and J.-H. Kim, "Thermoelastic damping effect of the micro-ring resonator with irregular mass and stiffness," *J. Sound Vib.*, vol. 369, pp. 168–177, May 2016.
[7] S. T. Hossain, S. McWilliam, and A. A. Popov, "An investigation on thermoelastic damping of high-Q ring resonators," *Int. J. Mech. Sci.*, vol. 106, pp. 209–219, Feb. 2016.
[8] C. Zener, "Internal friction in Solids. I. theory of internal friction in reeds," *Phys. Rev.*, vol. 52, no. 3, pp. 230–235, Aug. 1937.
[9] C. Zener, "Internal friction in solids II. General theory of thermoelastic internal friction," *Phys. Rev.*, vol. 53, no. 1, pp. 90–99, Jan. 1938.
[10] T. V. Roszhart, "The effect of thermoelastic internal friction on the Q of micromachined silicon resonators," in *Proc. IEEE 4th Tech. Dig. Solid-State Sensor Actuator Workshop*, Hilton Head Island, SC, USA, Jun. 1990, pp. 13–16.
[11] R. Lifshitz and M. L. Roukes, "Thermoelastic damping in micro- and nanomechanical systems," *Phys. Rev. B, Condens. Matter*, vol. 61, no. 8, pp. 5600–5609, Feb. 2000.

[12] S. Prabhakar and S. Vengallatore, "Theory of thermoelastic damping in micromechanical resonators with two-dimensional heat conduction," *J. Microelectromech. Syst.*, vol. 17, no. 2, pp. 494–502, Apr. 2008.
[13] J.-H. Kim and J.-H. Kim, "Mass imperfections in a toroidal micro-ring model with thermoelastic damping," *Appl. Math. Model.*, vol. 63, pp. 405–414, Nov. 2018.
[14] P. Li, Y. Fang, and J. Zhang, "Thermoelastic damping in microrings with circular cross-section," *J. Sound Vibrat.*, vol. 361, pp. 341–354, Jan. 2016.
[15] Y. Fang and P. Li, "Thermoelastic damping in thin microrings with two-dimensional heat conduction," *Phys. E: Low-Dimensional Syst. Nanostruct.*, vol. 69, pp. 198–206, May 2015.
[16] S. J. Wong, C. H. J. Fox, and S. McWilliam, "Thermoelastic damping of the in-plane vibration of thin silicon rings," *J. Sound Vib.*, vol. 293, nos. 1–2, pp. 266–285, May 2006.
[17] Y. Tai and N. Chen, "Thermoelastic damping in the out-of-plane vibration of a microring resonator with rectangular cross-section," *Int. J. Mech. Sci.*, vol. 151, pp. 684–691, Feb. 2019.
[18] S. Li, S. Chen, and P. Xiong, "Thermoelastic damping in functionally graded material circular micro plates," *J. Thermal Stresses*, vol. 41, nos. 10–12, pp. 1396–1413, Dec. 2018.
[19] Y. Sun and M. Saka, "Thermoelastic damping in micro-scale circular plate resonators," *J. Sound Vibrat.*, vol. 329, no. 3, pp. 328–337, Feb. 2010.
[20] S. Liu, Y. Sun, J. Ma, and J. Yang, "Theoretical analysis of thermoelastic damping in bilayered circular plate resonators with two-dimensional heat conduction," *Int. J. Mech. Sci.*, vol. 135, pp. 114–123, Jan. 2018.
[21] L. Yang, P. Li, Y. Fang, and H. Zhou, "Thermoelastic damping in bilayer microbeam resonators with two-dimensional heat conduction," *Int. J. Mech. Sci.*, vol. 167, Feb. 2020, Art. no. 105245.
[22] J. J. Bernstein, M. G. Bancu, E. H. Cook, M. V. Chaparala, W. A. Teynor, and M. S. Weinberg, "A MEMS diamond hemispherical resonator," *J. Micromech. Microeng.*, vol. 23, no. 12, Dec. 2013, Art. no. 125007.
[23] W. B. Bickford and S. P. Maganty, "On the out-of-plane vibrations of thick rings," *J. Sound Vibrat.*, vol. 108, no. 3, pp. 503–507, Aug. 1986.
[24] P. Chidamparam and A. W. Leissa, "Vibrations of planar curved beams, rings, and arches," *Appl. Mech. Rev.*, vol. 46, no. 9, pp. 467–483, Sep. 1993.
[25] S. Y. Lee and J. C. Chao, "Out-of-plane vibrations of curved non-uniform beams of constant radius," *J. Sound Vib.*, vol. 238, no. 3, pp. 443–458, Nov. 2000.
[26] J. E. Bishop and V. K. Kinra, "Elastothermodynamic damping in laminated composites," *Int. J. Solids Struct.*, vol. 34, no. 9, pp. 1075–1092, Mar. 1997.
[27] B. A. Boley and J. H. Weiner, *Theory of Thermal Stresses*. New York, NY, USA: Wiley, 1960.
[28] A. Duwel, R. N. Candler, T. W. Kenny, and M. Varghese, "Engineering MEMS resonators with low thermoelastic damping," *J. Microelectromech. Syst.*, vol. 15, no. 6, pp. 1437–1445, Dec. 2006.

YONGPENG TAI received the B.S. degree in mechanical manufacture and automation and the M.S. degree in mechanical design and theory from Nanjing Forestry University, China, in 2006 and 2009, respectively, and the Ph.D. degree in vehicle engineering from the School of Mechanical Engineering, Southeast University, Nanjing, China, in 2015. He is currently a Lecturer with Nanjing Forestry University. His current research interests include MEMS, control, vehicle dynamics, and fractional calculus.

NING CHEN received the B.S. degree in shipbuilding engineering from the Dalian University of Science and Technology, Dalian, Liaoning, China, in 1985, the M.S. degree in general mechanical from the Tianjin University, Tianjin, China, in 1991, and the Ph.D. degree in machinery manufacturing and automation from Southeast University, Nanjing, China, in 2009. He is currently a Professor with the College of Mechanical and Electronic Engineering, Nanjing Forestry University, Nanjing, China. His research activities focus on the vehicle dynamic and control, mechanical vibration analysis, nonlinear control theory, and fractional calculus theory and application.

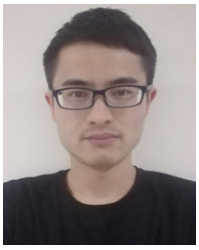

JUN XU received the B.E. degree in mechanical engineering from the Anhui University of Technology, Ma'anshan, China, in 2014. He is currently pursuing the Ph.D. degree with the School of Mechanical Engineering, Nanjing Forestry University, Nanjing, China. His research interests include the application of fractional calculus theory, modeling, and vibration control of dynamics of structures.

PU LI received the B.S. degree in mechanical design and manufacturing from the Shenyang University of Technology, Shenyang, Liaoning, China, in 1993, the M.S. degree in applied mechanics from the Nanjing University of Science and Technology, Nanjing, Jiangsu, China, in 1996, and the Ph.D. degree in machinery manufacturing and automation from Southeast University, Nanjing, China, in 2001. In 2002, he was a Research Assistant with The Hong Kong Polytechnic University, Hong Kong. He is currently a Professor with the School of Mechanical Engineering, Southeast University, Nanjing, China. His research activities focus on the mechanisms of energy dissipation in micro- and nano-resonators, such as thermoelastic damping and squeeze-film damping.